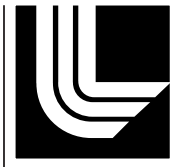

LAWRENCE
LIVERMORE
NATIONAL
LABORATORY

UCRL-JRNL-204477

High Repetition Rate Grazing Incidence Pumped X-ray Laser Operating at 18.9 nm

R. Keenan, J. Dunn, P.K. Patel, D.F. Price, R.F. Smith, and V.N. Shlyaptsev

May 11, 2004

Submitted to: Physical Review Letters

High Repetition Rate Grazing Incidence Pumped X-ray Laser operating at 18.9 nm

R. Keenan, J. Dunn, P.K. Patel, D.F. Price, R.F. Smith, and V.N. Shlyaptsev[1]

Lawrence Livermore National Laboratory, Livermore, CA 94550
[1]Department of Applied Science, University of California Davis-Livermore, Livermore, CA 94550

We have demonstrated a 10 Hz Ni-like Mo X-ray laser operating at 18.9 nm with 150 mJ total pump energy by employing a novel pumping scheme. The grazing incidence scheme is described, where a picosecond pulse is incident at a grazing angle to a Mo plasma column produced by a slab target irradiated by a 200 ps laser pulse. This scheme uses refraction of the short pulse at a pre-determined electron density to increase absorption to pump a specific gain region. The high efficiency inherent to this scheme allows a reduction in the pump energy where 70 mJ long pulse energy and 80 mJ short pulse energy are sufficient to produce lasing at a 10 Hz repetition rate. Under these conditions and by optimizing the delay between the pulses, we achieve strong amplification and saturation for 4 mm long targets.

Submitted for publication to Physical Review Letters 11 May 2004

When the x-ray laser was first demonstrated nearly 20 years ago [1] kilojoules of laser pump energy were required to generate a laser at ~20 nm. Two developments led to improved efficiency of these collisional pumped Ne- and Ni-like ion x-ray lasers. The first was the prepulse technique [2] where the target was irradiated with a low energy prepulse a few ns before the main pulse to form a preplasma. This gave better absorption of the main pulse, reduced density gradients and improved propagation and amplification of the x-ray laser beam along the plasma column. This allowed production of saturated x-ray lasers operating with pump energy as low as 30 J [3], outputs of a few mJs [4] and shorter wavelengths down to 5.8 nm [5]. The second advance came with the use of chirped pulse amplification (CPA) where smaller tabletop lasers could produce high irradiance in short pulses. Transient collisional excitation (TCE), where a nanosecond pre-pulse is followed by a short picosecond pulse pumping the population inversion, further reduced the laser pump to 10 J [6]. Saturated operation of these x-ray lasers has been demonstrated at 14.7 nm at a repetition rate of once every 4 minutes with less than 10 J pump [7] and at wavelengths as low at 7.3nm [8]. These achievements have used the transverse pumping geometry where the laser beams are incident at normal incidence and the laser energy is absorbed over a wide range of plasma densities. Recent work has shown further progress towards a high repetition rate soft x-ray laser based on longitudinal pumping with optical field ionization followed by collisional excitation [9]. High gain has been measured for Pd-like Xe at 41.8 nm and Ni-like Kr at 32.8 nm pumped with energy < 1 J and at a repetition rate of 10 Hz [10]. A longitudinal pumped Ni-like Mo x-ray laser at 18.9 nm has also been demonstrated [11], where a short pulse longitudinally pumps the inversion along a plasma column. This laser operated with a total pump energy of 150 mJ and produced a highly directional output but not in saturation. A saturated x-ray laser based on a table-top capillary discharge operating at 46.9 nm has produced millijoule level laser pulses at a repetition rate of 4 Hz [12] and has led to many applications.

We report the first demonstration of a novel pumping scheme using the excitation pulse incident on the plasma column at a grazing incidence angle to create an 18.9 nm Ni-like Mo 4*d* –

4*p* x-ray laser operating in saturation at 10 Hz repetition rate. This pumping geometry allows improved laser coupling efficiency into a pre-determined optimum gain region of the plasma by using refraction to turn the pump laser at an electron density below the critical density thus increasing the path length and absorption in this specific region of the plasma. This higher efficiency requires only a very low energy laser pump (~150 mJ), available at a 10 Hz repetition rate and represents more than an order of magnitude reduction in the pumping energy compared to the conventional transverse scheme. A systematic optimization of the pump parameters has been carried out showing strong lasing in targets of 4 mm in length for certain conditions. The x-ray laser gain is determined to be 60 cm^{-1} and appears to go into saturation for targets above 2 mm in length showing continued increase in intensity up to 4 mm. The x-ray laser exhibits small beam divergence and low deflection angles expected for the chosen gain region of ~10^{20} cm^{-3} and supports the physical basis for the novel geometry.

In the grazing incidence pumping (GRIP) scheme the same two stage pumping is used as in the conventional transient scheme but with a significant difference. A long pulse, 200 ps in this case, focused on a slab at normal incidence preforms a plasma column to create a tailored density profile. After a certain delay when the plasma conditions, particularly the electron density profile is correct, the short pulse is incident at a grazing angle to the target surface in a line focus. The short pulse beam is refracted in the plasma at a chosen electron density, well below critical, and is strongly absorbed. The required angle of incidence of the short pulse, measured relative to the target surface, is chosen to allow the laser pump to be refracted in the plasma. This is obtained from $\phi_r = \sqrt{n_{e0}/n_{ec}}$ where n_{eo} is the maximum density within the gain region and n_{ec} is the critical density for the optical pump [13]. This has several advantages that increase the laser coupling into the gain region. The grazing angle gives a longer path length to increase absorption within a specific plasma region. Refraction causes the short pulse to turn back into the gain region thus allowing the laser pump to traverse this region twice. The short pulse beam has an inherent traveling wave very close to the speed of light. For these reasons, a sub-20 nm x-ray laser should be able to be generated on a small, high-repetition rate laser.

To test the GRIP x-ray laser principle, the experiment was performed on an 800 nm wavelength, 100 fs Ti-Sapphire facility at the Lawrence Livermore National Laboratory. This laser typically produces a maximum of 300 mJ uncompressed laser energy per pulse at a repetition rate of 10 Hz. The energy was split with 33 % into the long pulse arm and 66 % into the short pulse arm. The long pulse, 200 ps in duration, was focused onto the Mo target at normal incidence as shown in Fig. 1 using a combination of a spherical and cylindrical lens. A total energy of 70 mJ was focused on target in a line of 5 mm long by 15 μm full width at half maximum (FWHM), at an intensity of 5×10^{11} W cm^{-2}. The short pulse arm was compressed under vacuum where a pulse length of 125 fs to 8 ps could be produced. The short pulse was focused to a line using a 91.4 cm focal length on-axis parabola tilted to produce the required grazing angle of incidence to the target as shown in Fig. 1. RADEX simulations [14] predicted that the optimum turning point of 10^{20} cm^{-3} electron density was required for the Ni-like Mo x-ray laser operating at 18.9 nm. From the above equation, this determined the 14^{o} angle of incidence considering the critical density of 1.74×10^{21} cm^{-3} for the 800 nm short pulse laser pump. The parabola produced a line focus 4 mm long by ~30 μm (FWHM) wide with a maximum energy on target of 80 mJ. The typical pulse duration of 1.5 ps on target gave an incident intensity of 4×10^{13} W cm^{-2}. This focusing geometry gave a traveling wave velocity of 0.98c. The long pulse arm was sent through a delay line that could adjust the separation of the two pulses from 0 – 1 ns. A surrogate optically transparent scatter film was placed at the target position to align the beams. The line foci were measured and overlapped using a laser achromat to image the target plane at high magnification onto a charge-coupled device (CCD) detector. The beams were incident onto a slab of polished Mo up to 4 mm in length.

The main diagnostic was an on-axis 1200 l/mm variable-spaced grating flat-field spectrometer, operating over a 10 – 25 nm wavelength range. The spectrometer was setup to image the target position, via a flat Ir-coated mirror, onto to a back-illuminated 1024 × 1024 pixel CCD positioned 1 m from the source. The detector had an angular view of 25 mrad in the horizontal direction and the spectrometer collected the central ~4 mrad in the vertical direction

determined by the effective height of the grating. Fiducial wires were placed close to the spectrometer entrance aperture and aligned relative to the target surface to give the deflection and beam divergence angles of the x-ray laser. Aluminum foils of 0.2 – 2 μm thickness were used as a light tight filter and to reduce the x-ray laser from saturating the CCD. The spectrometer was used to acquire the spectrum of a single shot. An on-axis soft x-ray Mo:Si multilayer-coated mirror imaging system, consisting of a 12.5 cm focal length mirror in combination with a 45^{o} mirror, was used to image the near-field pattern of the 18.9 nm Mo x-ray laser at 17× magnification onto a second back-illuminated CCD. Many laser near-field image x-ray laser shots could be recorded in one CCD frame by synchronizing the repetition rate of the laser with the CCD readout.

Some careful adjustment of the pumping conditions were required to achieve the soft x-ray laser line. Reducing the laser energy by more than 10% in each beam resulted in a strong fall in x-ray laser intensity. The optimized pump conditions were found to be a 1.5 ps short pulse delayed by 500 ps after the peak of the long pulse. Figure 2(a) shows a typical spectrum in a single shot for 150 mJ total energy incident on a 4 mm target. The wavelength dispersion direction is along the vertical axis while the horizontal axis gives the angular pointing of the x-ray emission perpendicular to the target. A lineout in the vertical direction, Fig. 2(b), shows intense output at 18.9 nm many orders of magnitude higher than any other feature. Figure 2(c) shows a narrow divergence angle of 3.6 mrad (FWHM) in the horizontal direction with a deflection angle of 3.2 mrad from the target. For the most intensely peaked shots the average deflection and divergence angles were 3 mrad and 4.5 mrad, respectively. The above formula can be applied very approximately to the measured peak of the deflection angles for the 18.9 nm x-ray laser and indicate the x-ray laser is emitted at an optimum electron density of $3 – 5 \times 10^{19}$ cm^{-3} and up to a maximum of 10^{20} cm^{-3}. This is consistent with the optimum maximum density chosen by the grazing incidence angle for the turning point of the short pulse beam. However, it should be noted that the incidence angle of laser pumping is not constant along the line focus

because of the range of beam angles from the focusing optic. This results in laser coupling to different electron densities.

The x-ray laser output was repeatable but was found to have some sensitivity to the overlap of the two line foci of the two beams, both with narrow widths. This was clearly observed in the near-field imaging, with up to 10 individual shots obtained spatially separated on the CCD image, where maximum x-ray laser output was observed for good overlap of the beams. In Fig. 3 we show the total output of the Ni-like Mo 18.9 nm line, recorded from the near-field imaging system, as a function of the delay between the short pulse and long pulse. The output is strongly peaked at a delay of 500 ps for a short pulse of 1.5 ps duration. The temporal window for the delay is extremely narrow at ~50 ps (FWHM) and different from recent characterization experiments of the Ni-like Pd x-ray laser pumped in the transverse geometry [15]. RADEX simulations indicate this high sensitivity to delay is attributed to the resultant plasma produced by the narrow focal width of ~15 μm (FWHM) and the relatively short pulse duration of 200 ps of the long pulse. Both of these laser parameters are several times smaller than previously described in transverse pumping designs and affect the inversion process for grazing incidence pumping. The plasma density gradients present at ~10^{20} cm^{-3} continue to relax with the onset of lasing at approximately 450ps after the peak of the long pulse, Fig. 3. The simulations show the plasma region containing the active medium Ni-like ions passes very quickly through the optimal density of ~10^{20} cm^{-3} selected by the grazing angle. At around 500ps the peak of Ni-like ion relative abundance passes through this density region and gives the strongest x-ray laser output. At longer delays of ~600-650ps the active ions have moved away from the target and the pumping region while the overall electron density has dropped substantially with reduced laser coupling. The modeling shows good agreement with the observed peak of the delay for best lasing conditions. The predicted time history after the peak and the width of the time window for lasing is very sensitive to the initial long pulse pump conditions and is under further study.

Ni-like Mo experiments have shown laser action in recent years to varying degrees with small pump energies [11, 16, 17]. An important objective in this work was to determine the gain

for the GRIP scheme with traveling wave pumping and show continued increase in x-ray laser output as a function of target length. Single shots were taken with data recorded through imaging and on the spectrometer for lengths up to 4 mm, Fig. 4. It should be noted the x-ray laser intensity increases by approximately three orders of magnitude from the threshold of detection for 1.5 mm targets to the maximum of 4 mm. The x-ray laser output continues to increase at the longest targets but at a lower rate. The highest gain is determined to be 60 cm^{-1} for targets up to 2 mm with no output detected for targets below 1.5 mm. For a 2 mm target the gain length (GL) product of 12 is achieved with the output rolling over indicating a saturation-like behavior. The intensity is higher by a further factor of 20 for targets up to 4 mm long which determines an upper limit of the GL~15 which would be into saturation. For the laser conditions studied here the gain region cross-section is fairly small ~9 × 20 μm^2 and the mean electron density is expected to be in the range of 4 – 8 × 10^{19} cm^{-3}. RADEX simulations indicate that for 4 mm target lengths and the relatively low electron density, refraction should not be a significant problem for the x-ray laser propagation along the plasma column. For the above beam size and assuming ~2 ps pulse duration the saturation intensity of ~0.5 – 1.0 × 10^{10} W cm^{-2} would be achieved with an output of approximately 10 – 20 nJ. The output of this x-ray laser could be substantially improved by pumping longer targets and generating a larger gain region by widening the line foci on the long and short pulse. Additional details of the grazing incidence scheme, including the RADEX computed hydrodynamic parameters, refraction of laser radiation, and detailed analysis of the scheme's advantages and disadvantages will be described in a separate publication.

In conclusion the new grazing incidence pumping scheme has allowed lasing for Ni-like Mo at 18.9 nm to be demonstrated with only 150 mJ total energy on target with a pump laser operating at 10 Hz. The angle of incidence of the short pulse is chosen such that short pulse experiences the optimum maximum electron density for pumping the inversion and is then refracted back into the gain region. This allows pumping at much lower energy as the short pulse is absorbed more effectively in the density region where gain occurs. High gain has been inferred

at short target lengths. The sensitivity to delay between the long pulse and short pulse is in part due to the available long pulse pump energy determining the line focus parameters. These are the first experiments to utilize this new geometry and it is expected that further improvements will be made in the near future. The grazing incidence pumping is another step forward in the improvement in efficiency of x-ray laser that will lead to new applications that require high average power at a high repetition rate and low pump energy.

The continued support of A. Osterheld is greatly appreciated. We thank J. Nilsen and T.W. Barbee, Jr. for the use of the multilayer optics. We acknowledge the technical contributions of J. Boyett, R. Van Maren, C. Bruns, R. Berry and J. Hunter. Work performed under the auspices of the US Department of Energy by the University of California Lawrence Livermore National Laboratory under Contract No. W-7405-Eng-48 and in part by funding from the National Science Foundation through the Center for Biophotonics, an NSF Science and Technology Center, managed by the University of California, Davis, under Cooperative Agreement No. PHY 0120999.

References:

1. D.L. Matthews et al, Phys. Rev. Lett. **54**, 110-113, (1985).
2. J. Nilsen, B. MacGowan, L. B. DaSilva, and J. C. Moreno, Phys. Rev. A **48**, 4682-4685 (1993).
3. R. Tommasini, F. Löwenthal and J. E. Balmer, Phys. Rev. A **59**, 1577-1581 (1999).
4. B. Rus, T. Mocek, A.R. Prag, M. Kozlova, G. Jamelot, A. Carillon, D. Ros, D. Joyeux and D. Philippou, Phys. Rev. A **66**, 063806 1-12 (2002).
5. R. Smith, G.J. Tallents, J. Zhang, G. Eker, S. McCabe, G.J. Pert, and E. Wolfrum, Phys. Rev. A **59**, R47-R50 (1999).
6. P.V. Nickles, V.N. Shlyaptsev, M. Kalachnikov, M. Schnurer, I. Will and W. Sandner, Phys. Rev. Lett. **78**, 2748-2751 (1997).
7. J. Dunn, Y. Li, A.L. Osterheld, J. Nilsen, J.R. Hunter, V.N. Shlyaptsev, Phys. Rev. Lett. **84**, 4834-4837 (2000).
8. R. E. King, et al, Phys. Rev. A, **64** 053810 1-12 (2001).
9. B.E. Lemoff, G.Y.Yin, C.L.Gordon III, C.P.J. Barty, S.E. Harris, Phys. Rev. Lett. **74**, 1574-1577 (1995).
10. S. Sebban, et al, Phys. Rev. Lett. **86**, 3004-3007, 2001; S. Sebban, et al, Phys. Rev. Lett. **89**, 253901 1-4 (2002).
11. T. Ozaki, et al, Phys. Rev. Lett. **89**, 253902 1-4 (2002).
12. C. D. Macchietto, B. R. Benware, J. J. Rocca, Opt. Lett. **24**, 1115-1117 (1999).
13. V. N. Shlyaptsev et al., Proc. SPIE Int. Soc. Opt. Eng. **5197**, 221 (2003); V.L. Ginzburg, *Propagation of Electromagnetic Waves in Plasma*, (Addison–Wesley, Reading, 1964).
14. N.G.Basov, V.P.Avtonomov, Yu.V.Afanasiev et al, J. Sov. Laser Research **10**, 1 (1989).
15. R.F. Smith et al, Proc. SPIE Int. Soc. Opt. Eng. **5197**, 155 (2003).
16. R. Li, Z.Z. Xu et al., Journal de Physique IV **11** (PR2), 27-34 (2001).
17. R.Tommasini, J. Nilsen, and E.E. Fill, Proc. SPIE Int. Soc. Opt. Eng. **4505**, 85 (2001).

Figure Captions

Figure 1 Experimental setup showing grazing incidence pumping of short pulse laser beam.

Figure 2 (a) Soft x-ray spectrum from on-axis flat-field spectrometer. The two vertical lines are the fiducial wires used to calibrate the x-ray laser deflection angle relative to the target surface. (b) (Right) Intensity lineout showing strong lasing at 18.9 nm from Ni-like Mo $4d - 4p$ transition. (c) Horizontal lineout showing narrow angular profile of x-ray laser beam.

Figure 3 Measured x-ray laser intensity (closed circles) as a function of time delay between the long pulse and short pulse for a 1.5 ps short pulse together with RADEX modeling (solid line) under similar laser pumping conditions.

Figure 4 X-ray laser intensity *versus* target length showing strong output with increasing target length. A gain of 60 cm^{-1} is inferred from 1.5 to 2 mm targets.

Fig. 1

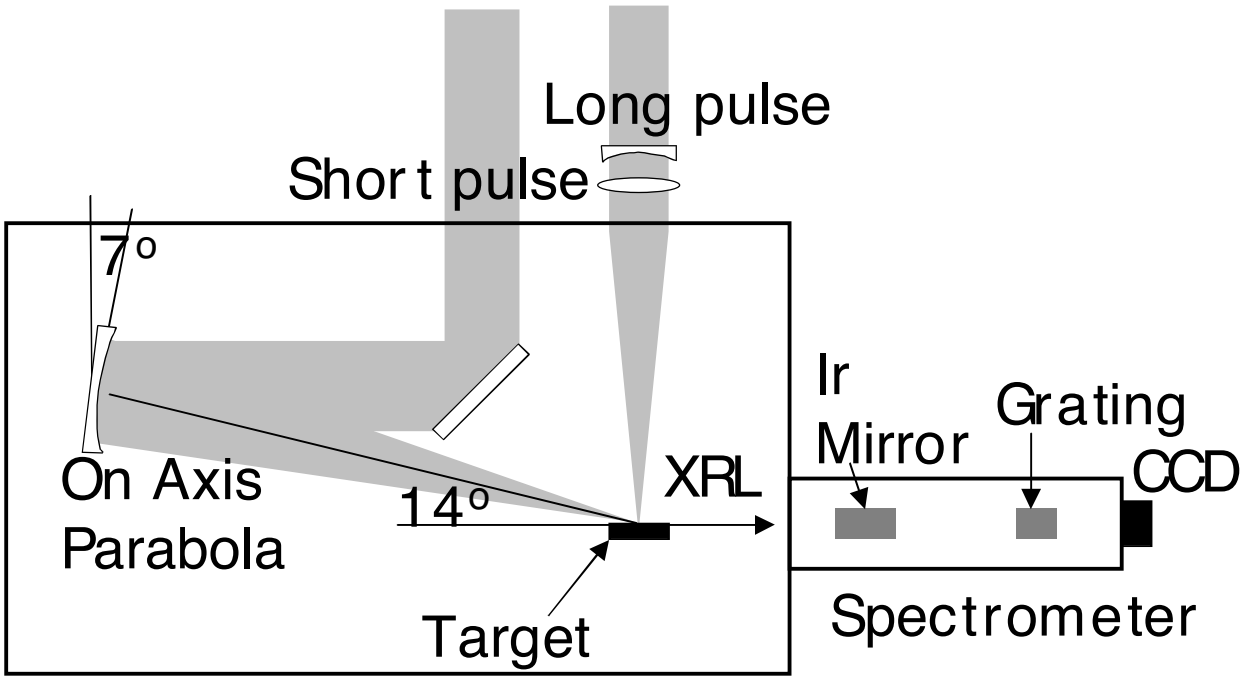
Long pulse
Short pulse
7°
On Axis
Parabola
14°
XRL
Target
Ir
Mirror
Grating
CCD
Spectrometer

Fig. 2

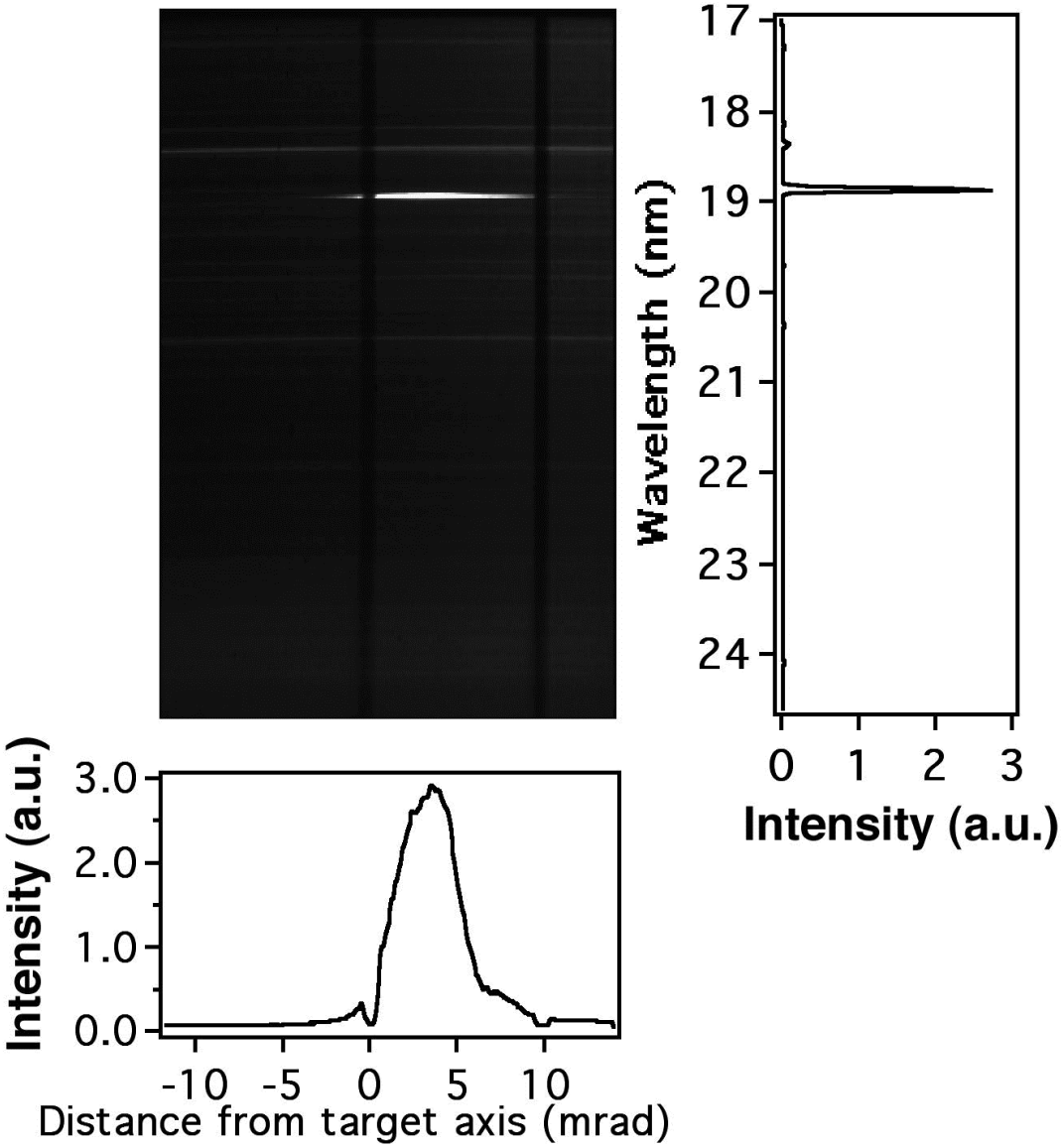
17
18
19
20
21
22
23
24
Wavelength (nm)
0
1
2
3
Intensity (a.u.)
3.0
2.0
1.0
0.0
Intensity (a.u.)
-10
-5
0
5
10
Distance from target axis (mrad)

Fig. 3

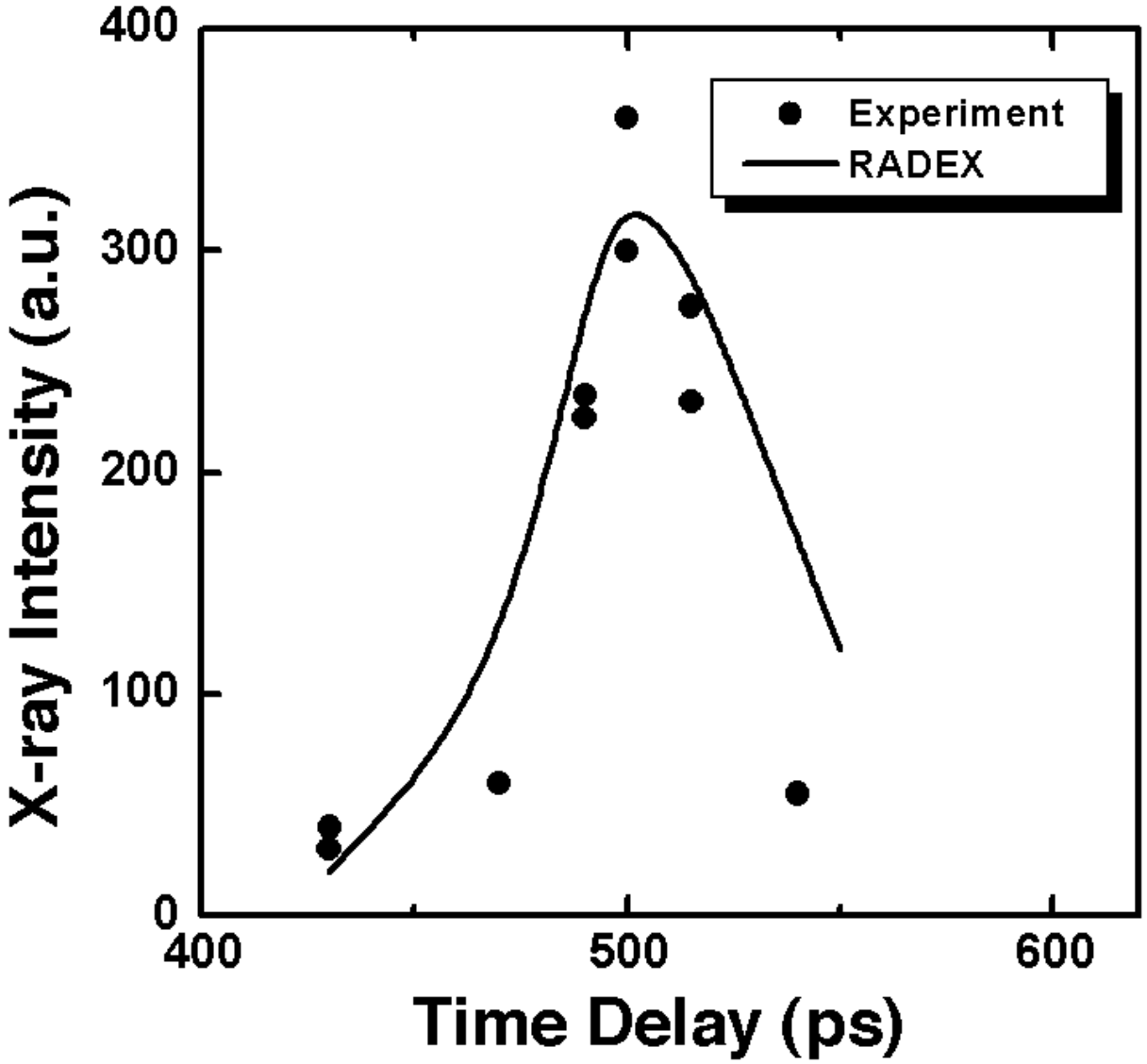
Experiment
RADEX
X-ray Intensity (a.u.)
Time Delay (ps)
0
100
200
300
400
400
500
600

Fig. 4